Biochemical and Biophysical Research Communications 461 (2015) 70–75

Contents lists available at ScienceDirect

Biochemical and Biophysical Research Communications

journal homepage: www.elsevier.com/locate/ybbrc

Molecular imaging of inflammation in the ApoE -/- mouse model of atherosclerosis with IodoDPA

Catherine A. Foss [a, *, 1], Djahida Bedja [b, d, 1], Ronnie C. Mease [a], Haofan Wang [a, 2], David A. Kass [b], Subroto Chatterjee [c], Martin G. Pomper [a]

[a] Russell H. Morgan Department of Radiology and Radiological Science, Johns Hopkins University School of Medicine, Baltimore, MD 21287, USA
[b] Department of Medicine, Division of Cardiology, Johns Hopkins University School of Medicine, Baltimore, MD 21287, USA
[c] Department of Pediatrics, Johns Hopkins University School of Medicine, Baltimore, MD 21287, USA
[d] Faculty of Medicine and Health Sciences, Macquarie University, Sydney, Australia

ARTICLE INFO

Article history:
Received 18 March 2015
Available online 6 April 2015

Keywords:
Arteriosclerosis
Macrophages
Coronary artery disease
TSPO imaging
oxLDL

ABSTRACT

Background: Atherosclerosis is a common and serious vascular disease predisposing individuals to myocardial infarction and stroke. Intravascular plaques, the pathologic lesions of atherosclerosis, are largely composed of cholesterol-laden luminal macrophage-rich infiltrates within a fibrous cap. The ability to detect those macrophages non-invasively within the aorta, carotid artery and other vessels would allow physicians to determine plaque burden, aiding management of patients with atherosclerosis.

Methods and results: We previously developed a low-molecular-weight imaging agent, [^{125}I]iodo-DPA-713 (iodoDPA), which selectively targets macrophages. Here we use it to detect both intravascular macrophages and macrophage infiltrates within the myocardium in the ApoE -/- mouse model of atherosclerosis using single photon emission computed tomography (SPECT). SPECT data were confirmed by echocardiography, near-infrared fluorescence imaging and histology. SPECT images showed focal uptake of radiotracer at the aortic root in all ApoE -/- mice, while the age-matched controls were nearly devoid of radiotracer uptake. Focal radiotracer uptake along the descending aorta and within the myocardium was also observed in affected animals.

Conclusions: IodoDPA is a promising new imaging agent for atherosclerosis, with specificity for the macrophage component of the lesions involved.

1. Introduction

Atherosclerosis accounts for the majority of cardiovascular and cerebrovascular disease worldwide [1,2]. It is characterized by thickening and sclerosis of the vessel walls due to the presence of cholesterol-rich plaques and calcification [3]. Plaques are generated in part by infiltration of monocytes due to inflammation propagated by the dynamic interplay between the endothelial cells and resident macrophages [4]. Those macrophages further promote collagen remodeling by recruiting fibroblasts [5] and also catalyze deposition of mineralized calcium, also resulting in arteriosclerosis [6]. High levels of dietary and/or endogenous cholesterol-bound, low-density lipoprotein (LDL), along with increased oxidative stress, [7] directly contribute to an increase in oxidized LDL levels in blood. Oxidized LDL (oxLDL) is associated with progression of atherosclerosis and plaque vulnerability[8]. OxLDL binds to specific receptors, including lectin-like oxidized LDL receptor (LOX-1), which reside on the surface of endothelial cells [9]. OxLDL also binds to scavenger receptors of class A, B and C, including macrosialin (CD68) [10], which is expressed primarily by macrophages and other phagocytes [11]. These oxLDL-binding scavenger receptors are directly associated with the formation of plaque-forming foam cells [8,12]. Because cholesterol transport and foamy macrophages are integral to the formation of atherosclerotic plaques, they have been targeted for imaging to visualize plaque and as a means to molecularly monitor anti-inflammatory interventions such as the use of statins [13].

Abbreviations: iodoDPA, iodo-DPA-713; SPECT, single-photon emission tomography; TSPO, translocator protein; HFHC, high fat high cholesterol.

* Corresponding author. Johns Hopkins University, 1550 Orleans St, CRB2 493, Baltimore, MD 21287. Fax: +1 410 614 3147.
E-mail address: cfoss1@jhmi.edu (C.A. Foss).

[1] Equal contribution.
[2] Present address: U.S. Food and Drug Administration, Rockville, MD, USA.

http://dx.doi.org/10.1016/j.bbrc.2015.03.171
0006-291X/

The LOX-1 receptor has previously been targeted to image affected endothelium directly within plaques in the ApoE -/- mouse model by radiolabeling anti-LOX-1 antibody-targeted liposomes with ^{99m}Tc-99m [14]. Those efforts led to visualization of lesions within the aortic arch but exhibited high hepatic uptake of radiolabeled liposomes, which prevented visualization of lesions within the descending aorta. OxLDL itself has also been targeted for imaging, using radiolabeled anti-oxLDL antibodies and SPECT [15] in a rabbit model of atherosclerosis, and a radioiodinated peptide specific for oxLDL [16] has also been developed. TSPO, the translocator protein [17], binds cholesterol on the mitochondrial membrane and is found in all steroidogenic tissues including the heart and liver. TSPO is upregulated in activated monocytes and macrophages. TSPO has been targeted to image neuroinflammation [18–20], cancer [17] and inflammation associated with coronary artery disease (CAD) [21,22]. Here we use [^{125}I]iodo-DPA-713 (iodoDPA), a second generation TSPO radioligand we previously developed to image inflammation in the periphery [35], to target plaque-associated macrophages specifically. We show that the mechanism by which iodoDPA binds to plaques is related to TSPO-independent trapping within phagocytic cells [23].

2. Materials and methods

2.1. Animals

Animal procedures were performed in accordance with the regulations of the Johns Hopkins Animal Care and Use Committee (ACUC). Twelve-week-old male apolipoprotein E-deficient (ApoE -/-) (stock number 092052), and age-matched male C57Bl/6 mice were purchased from the Jackson Laboratories (Bar Harbor, ME). Mice were housed in a pathogen free facility with access to food and water *ad libitum* and maintained on a 12 h light/dark cycle. Mice were divided into three groups, one of which consumed a high fat, high cholesterol diet (HFHC) of 4.5 kcal/g, 20.0% fat, and 1.25% cholesterol (D12108C, Research Diet Inc., New Brunswick, NJ) for up to 36 weeks. Additional groups of ApoE -/- and C57Bl/6 mice were fed standard, autoclaved diet (Teklad 8604 Rodent Diet, Harlan Laboratories, Frederick, MD). At the end of the study mice were euthanized by CO_2 asphyxiation or cervical dislocation under sedation. Tissues were harvested after either 24 (40 weeks of age) or 36 (57 weeks of age) weeks on diet for molecular imaging and histopathologic studies.

2.2. Transthoracic echocardiography

Trans-thoracic echocardiography was performed in conscious mice using the 2100 Visualsonic ultrasound system (Toronto, Ontario, Canada), equipped with an ultra-high frequency linear array micro-scan transducer of 30–40 MHz [24]. Measurements were performed according to the guidelines set by the American Society of Echocardiography. For each mouse, three to five values for each measurement were obtained and averaged for evaluation. M-mode echocardiograms were acquired to verify location of plaques within individual mice [24].

The aorta was viewed in two-dimensional (2-D) mode in the parasternal long axis view of the LV. From that view the ascending aortic (AsAo) diameters, including the internal and the external diameter, were measured and were used to estimate the intima media thickness (IMT) [23,25].

2.3. Synthesis and administration of imaging agents

IodoDPA was synthesized as described previously [26] and batches used ranged from 70.3 to 77.7 GBq/mmol (1900–2100 Ci/mmol) in specific radioactivity. The radiotracer was formulated in 10% ethanol in PBS, pH 7.4 and was injected as a 100 μL intravenous bolus through the tail vein. DPA-713-IRDye680LT was formulated in 10% DMSO in PBS, pH 7.5, as previously described [35]. The 100 μL volume of DPA-713-IRDye680LT was always combined with a 100 μL volume of BoneTag800™ (LI-COR Biosciences, Lincoln, NE), formulated in 100% PBS, pH 7.4 prior to bolus tail vein injection.

2.4. SPECT imaging

One representative mouse from each group at 26 wk post-diet (two mice with plaques, one without) and at 35 wk post-diet (two mice with plaques, one without) was injected with an equal amount of radiotracer (31.4 ± 0.4 MBq (849 ± 11 μCi), 26 wk on diet and 85.1 ± 3.5 MBq (2.3 ± 0.95 mCi), 35 wk on diet). Mice were scanned 24 h later by SPECT-CT. Mice had free access to their accustomed diets and water during this period. Mice were anesthetized using 3% isoflurane in oxygen (2 L/min) and were maintained using 2% isoflurane in oxygen while being scanned in pairs using a Gamma Medica X-SPECT scanner (Gamma Medica Ideas, Northridge, CA) equipped with two medium energy pinhole (0.5 mm diameter) collimators. Each SPECT scan was composed of 64 projections for 55 (26 wk mice) or 45 (35 wk mice) seconds per projection to accommodate the difference in injected dose between groups. A computed tomography (CT) scan was performed for anatomic co-registration and utilized a 512 slice protocol at 50 kV beam potential. CT and SPECT data were reconstructed and co-registered using the manufacturer's software and the data were displayed and analyzed using AMIDE (http://amide/sourceforge.net).

2.5. Near-infrared fluorescence imaging

One representative mouse from each group was injected concurrently with DPA-713-IRDye680LT and BoneTag800CW™. Mice underwent a 24 h uptake period prior to imaging using a Pearl Impulse Imager (LI-COR Biosciences, Lincoln, NE). Mice were sacrificed by cervical dislocation prior to exposing the heart and lungs. Images were acquired using 680 nm (excitation)/710 nm (emission) and 790/800 nm band pass filters as well as a white light photograph. Images were displayed using the manufacturer's software (Pearl Impulse Software v. 2.0). *In situ* photographs of the heart and ascending aorta were captured prior to collection for histologic examination.

2.6. Epifluorescence microscopy

Tissues from mice injected with DPA-713-IRDye680LT and BoneTag800CW™ were collected, fixed in neutral-buffered formalin for 48 h, grossed and embedded in paraffin prior to sectioning to 4 μm slices onto charged glass slides. The slides were de-paraffinized and then immediately probed with a solution of PBS, pH 7.5 containing 10% fetal bovine serum (FBS) (Gibco, Grand Island, NY) and anti-CD68 antibody (Abcam, Cambridge, MA, ab955, 1:67) for 1 h at room temperature. The slides were then washed twice for 5 min each with PBS and then probed with goat anti-mouse secondary antibody-fluorescein conjugate (Abcam, ab97022, 1:250) in PBS for 30 min at room temperature. Following aspiration of the secondary antibody solution, the slides were then exposed to Hoechst 33342 dye for 1.5 min (Invitrogen, Grand Island, NY USA, H3570, 1:1000 in PBS). The slides were then washed twice more with PBS for 5 min each prior to adding mounting medium (Dako Faramount Aqueous Mounting Medium, Carpenteria, CA) and a glass coverslip. The slides were then immediately viewed using a Nikon 80i upright epifluorescence microscope equipped

with a Nikon DS-Qi1Mc darkfield CCD camera and excited by a Nikon Intensilight C-HGFI lamp. All images were recorded and processed using Nikon Imaging Software Elements.

3. Results

3.1. Fluorescent analog DPA-713-IRDye680LT co-localizes with vascular and infiltrating myocardial macrophages in ApoE -/- mouse atherosclerotic plaques

Fig. 1 shows four views of an ApoE -/- mouse heart from an animal that was fed a HFHC diet for 36 wk, with white light only in panel **1A**, activated macrophages in the aortic arch (red, AsAo arrow) and brachialcephalic artery (BCA arrow) in **1B**, co-morbid mineralized calcium deposits in the aortic root (green, solid arrows) and cut ribs (green, dotted arrows) in **1C** and combined channels showing proximal and overlapping calcium mineral (green) and inflammation (red) in **1D**. An uninjected (no probe) C57bl/6 mouse (**1E**) and a C57bl/6 control mouse injected with both probes (**1F**) are also shown for comparison of both no inflammation and background tissue fluorescence (**1E**). Panel **E** shows no autofluorescence from an uninjected mouse and no visible DPA-713-IRDye680LT uptake in the age-matched C57bl/6, with only a small spot of BoneTag800CW™ uptake in the ascending aorta. Focal uptake of DPA-713-IRDye680LT (red) and BoneTag800CW™ (green) were matched with pre-sacrifice echocardiography showing the presence of both plaque and mineralized calcium in *ex vivo* images of excised heart and descending aorta. C57bl/6 mice showed a small amount of inflamed plaque without calcium at the aortic root (Fig. 2A1–3). ApoE -/- mice fed a standard diet showed a small amount of inflamed plaque at the aortic root as well as mineralized calcium (Fig. 2B1-3) while ApoE -/- mice fed a HFHC diet for 36 wk showed inflammation within the aortic root and descending aorta accompanied by calcium deposits within the aortic root (Fig. 2C1-3).

Following *ex vivo* macroscopic imaging of hearts with descending aortas, these tissues were then sectioned and subsequently co-stained with anti-CD68 antibody to delineate macrophages and Hoechst 33342 (cell nuclei) (Fig. 3). These markers were applied to verify cell-type specificity of fluorescent probe trapping in diseased artery. The red channel depicts *ex vivo* trapped DPA-713-IRDye680LT as well as brightly autofluorescent red blood cells trapped in the remaining lumen. The green anti-CD68 channel shows CD68 + macrophages within the plaque, autofluorescent red blood cells in the lumen and wavy autofluorescent collagen within the vessel walls. A magnified view of the cellular portion of the plaque in the lower, right panel (white parenthesis) shows numerous macrophages (white arrows) that are CD68+ and retain DPA-713-IRDye680LT (co-localizing as orange) close to the nucleus.

3.2. IodoDPA SPECT detects inflammation in heart, ascending and descending aorta

Four plaque-bearing mice and two healthy mice (n = 2 plaque-bearing, n = 1 healthy at 24 wk on diet and another group at 36 wk post-diet (n = 2 plaque-bearing, n = 1 healthy) were imaged using iodoDPA SPECT to assess whether inflammatory lesions could be non-invasively localized with high contrast amid normal tissues, including the adjacent TSPO-expressing heart [27,28]. Fig. 4 shows SPECT slices in three orientations with a selected lesion highlighted inside the red crosshairs for each mouse. Sagittal sections are shown for the 24 wk mice, which are from another cohort. All mice displayed foci of inflammation within ascending and/or descending aorta. All mice displayed normal radiotracer uptake and retention within macrophage-rich brown fat [29,30] (BF) and nearby cervical, brachial and axillary lymph nodes. The TSPO-rich heart remains dark except for focal uptake in the heart of ApoE -/- mice fed a standard diet. ApoE -/- mice fed a standard diet also develop inflammation and vascular plaques but at lower frequency than those fed a HFHC diet. As anticipated, individual mice varied in the

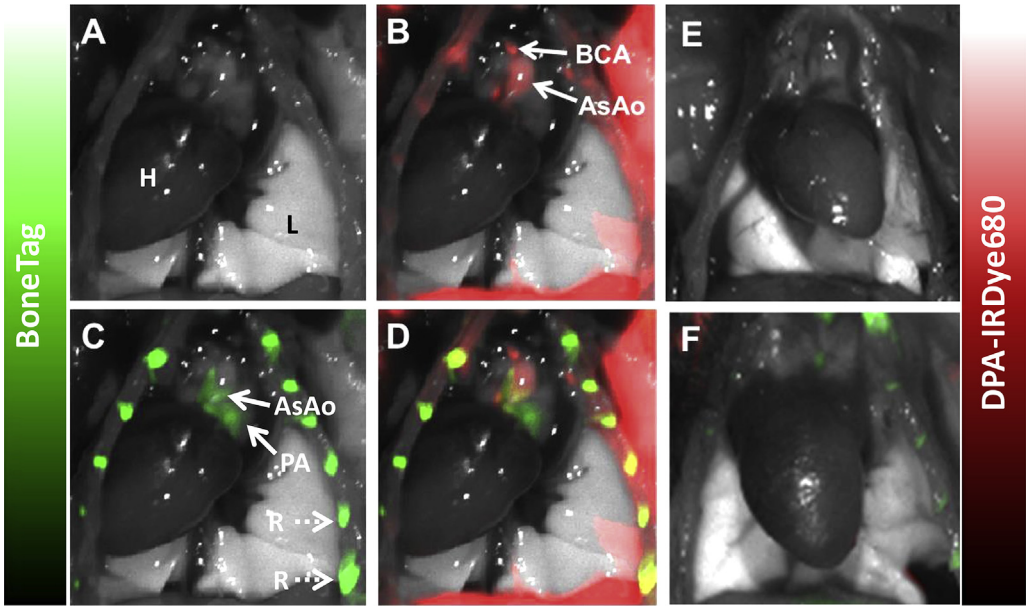

Fig. 1. Near-IR fluorescence imaging of mineralized calcium and activated macrophages in mouse vessels. A 35 week old ApoE KO (ApoE -/-) male mouse fed a high fat, high cholesterol (HFHC) diet was co-injected with BoneTag800™ and DPA-713-IRDye680LT and imaged 24 h later, after sacrifice. (**A**) Heart (H) and lungs (L); (**B**) Inflammation in the aortic arch [ascending aorta (AsAo) and the brachiocephalic artery (BCA)]; (**C**) Accumulation of mineralized calcium shown by BoneTag800 in the large vessels/vessel (AsAo) and ribs (green); (**D**) Overlay of **B** and **C**. (**E**) Heart and lungs from an age-matched C57bl/6 mouse injected with no compound; (**F**) Another age-matched C57bl/6 mouse injected with BoneTag800™ and DPA-713-IRDye680LT. The latter likely shows a small accumulation of calcium deposits which is due to a normal aging process in the C57bl/6 mouse on normal chow diet. (For interpretation of the references to colour in this figure legend, the reader is referred to the web version of this article.)

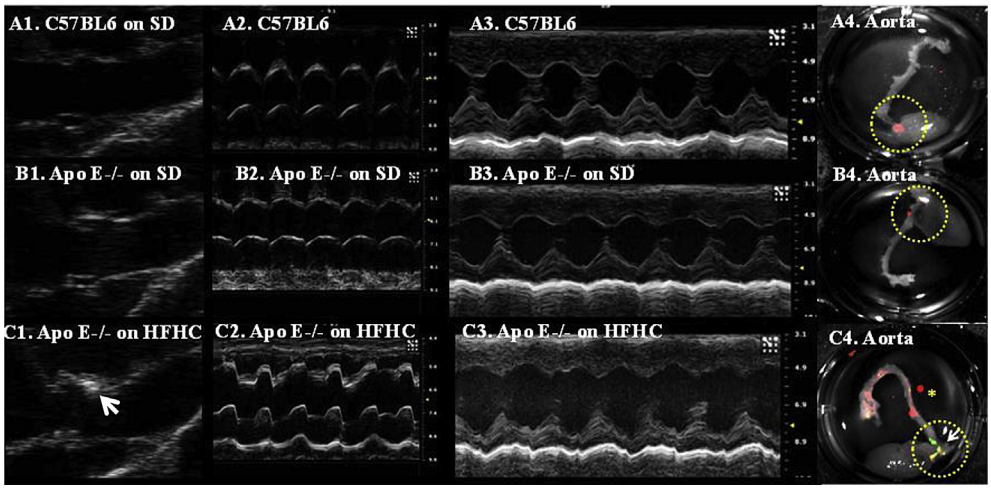

Fig. 2. Representative 2D (**A1**, **B1**, **C1**) and M-mode echocardiograms (**A2**, **B2**, **C2**) of the aorta with corresponding near-IR fluorescence imaging of murine heart and aorta (**A3**, **B3**, **C3**). These data are from male C57bl/6 (**A**) and ApoE -/- (**B**) fed standard diet (SD), and (**C**) ApoE -/- fed HFHC at the age of 36 wk. Ultrasonography of ApoE -/- fed HFHC confirms a significant increase in aortic wall thickness, plaque and calcium deposition (arrow) as compared to control C57bl/6 and ApoE -/- (**B**) fed a SD (**C1**, **B1**), which is consistent with the overlay of activated macrophages and mineralized calcium seen in **C3**. The abnormal motion of the aortic wall observed by M-mode (**C2**) in ApoE -/- fed a HFHC diet is due to calcium accumulation, which is confirmed by the uptake of BoneTag™ calcium probe (green) in **C4**. The small amount of inflammation (red) detected by DPA-713-IRDye680LT probe (**A3**, **B3**) in C57bl/6 and ApoE -/- fed a SD may be due to normal aging as it was not accompanied by calcium probe uptake (green). (For interpretation of the references to colour in this figure legend, the reader is referred to the web version of this article.)

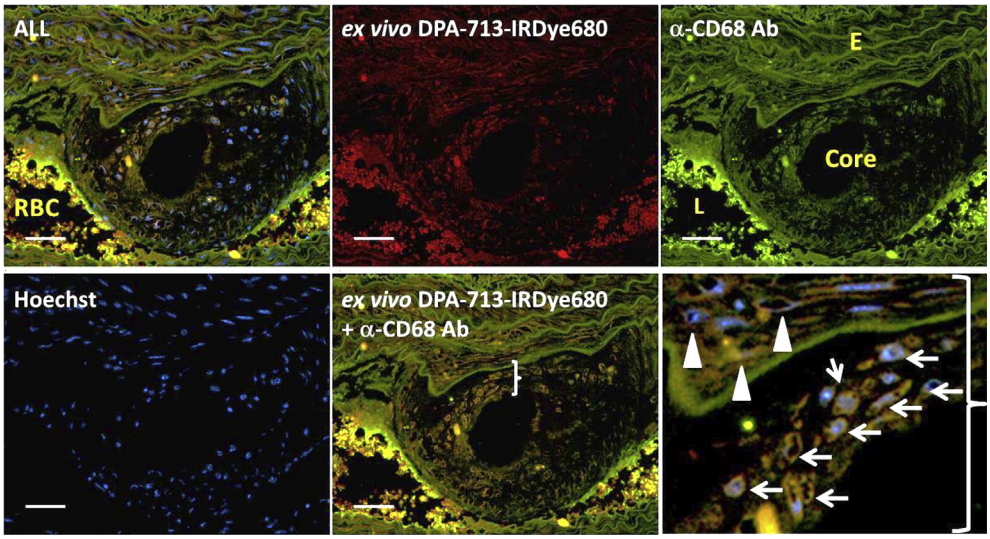

Fig. 3. Immunfluorescence micrograph of murine coronary vessel showing co-localization of ex vivo DPA-713-IRDye680LT with CD68 positive macrophages within plaque wall. "L" denotes the lumen of the vessel. *RBC* denotes autofluorescent red blood cells. *E* denotes autofluorescent elastin. *Core* denotes the acellular core of the plaque. The white parenthesis denotes the region expanded in the last panel. Arrows denote plaque-associated macrophages and arrowheads denote macrophages in the arterial wall, many of which appear apoptotic. Scale bar = 50 μm.

degree of plaque burden, and SPECT scans correctly revealed actual plaque burden regardless of dietary group. SPECT-CT scans are available for individual inspection in Supplementary Figs. 1–4.

4. Discussion

We report a method to detect macrophage-specific inflammation within atherosclerotic plaques using iodoDPA SPECT in ApoE -/- mice. We have demonstrated ultrasound confirmed co-localization of radiotracer SPECT signal with plaque in ascending aorta (Fig. 4). We have also demonstrated co-localization of the fluorescent agent, DPA-713-IRDye680LT, with plaque in whole-mount tissues imaged *ex vivo* (Figs. 1 and 2) as well as specific co-localization with CD68-expressing macrophages within inflamed plaques imaged by epifluorescence microscopy (Fig. 3). While DPA-713 is reported as a ligand of TSPO [19,26], we previously determined that analogs of DPA-713 such as [^{125}I]iodo-DPA-713 and DPA-713-IRDye680LT [31], become specifically sequestered *in vivo* within CD68-expressing phagocytes after a 24 h uptake period. We additionally demonstrated previously that after a 24 h uptake period, iodo-DPA-713 and DPA-713-IRDye680LT clears from healthy TSPO-containing tissues such as heart and lung [31], permitting imaging of inflammation within a context of low radiotracer background signal.

IodoDPA SPECT imaging of mice revealed focal vascular and cardiac uptake of radiotracer within both ApoE -/- mouse groups showing very little uptake within C57bl/6 control mice, reflecting individual severity of phenotype. All scans provided images free from competing heart, liver and normal lung uptake in contrast to scans typically seen using 2′-deoxy, 2′-[^{18}F]fluoroglucose (FDG)

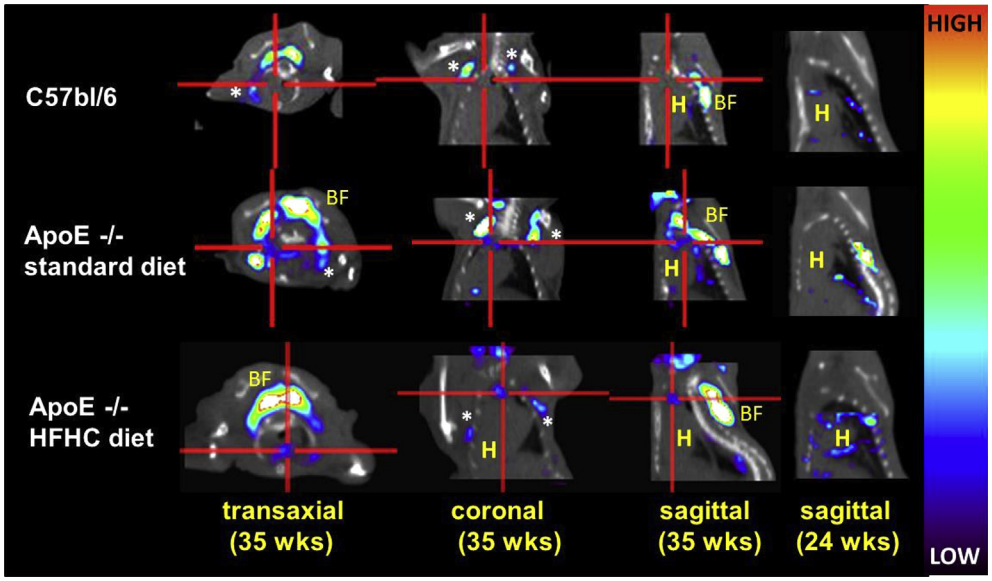

Fig. 4. [^{125}I]iodo-DPA-713 SPECT-CT imaging at 24 h post-injection of activated macrophages in atherosclerotic plaques at 36 and 24 wk on-diet (40 and 36 wk of age). The 24 and 36 wk mice are different mice. A selected lesion is shown in all three views using the red crosshairs. Age-matched C57bl/6 is compared with ApoE -/- on normal diet and ApoE -/- on high fat, high cholesterol diet (HFHC). Lesions in and around the heart (H) can clearly be seen as well as in ascending (AsAo) and descending aorta. Brown fat (BF), which is rich in macrophages, is clearly seen as well as axillary lymph nodes (*). (For interpretation of the references to colour in this figure legend, the reader is referred to the web version of this article.)

PET. Many other TSPO-specific radioligands are currently in preclinical or clinical use, but tend to employ short-lived radionuclides, such as ^{11}C (20 min physical half-life) and ^{18}F (110 min). As such they are unable to accommodate the 24 h uptake time needed to achieve selective trapping in macrophages to provide higher signal-to-noise clarity in otherwise normal tissues. All TSPO-specific radiotracers bind to TSPO-rich cardiac, lung and liver and are typically restricted to interrogation of tissues with low endogenous TSPO expression, such as the brain [19,32]. However a recent report described the use of [^{18}F]DPA-714 in rheumatoid arthritis (RA), where minimal background uptake would be expected [33], as well as the use of [^{18}F]PBR28 to image another rodent model of RA [34]. To date, only one TSPO-targeted radiotracer has been used clinically to delineate atherosclerotic plaque, namely, [^{11}C](*R*)-PK11195 [22]. In that study [^{11}C](*R*)-PK11195 PET-CT was used to delineate inflamed, symptomatic stenosis within the carotid arteries of patient volunteers. Another study using the same radiotracer and method imaged inflammation in the arteries of patients with vasculitis [35] and found radiotracer uptake in the ascending aorta and carotids to be higher among the patients with vasculitis than among healthy controls. Atherosclerosis and other vascular inflammatory pathologies occur throughout the body and a need exists to image those sites of inflammation sensitively and specifically, especially in proximity to TSPO-rich and metabolically active tissues like heart, liver and kidneys [36]. IodoDPA SPECT or PET may provide clinically translatable macrophage-specific imaging throughout the body due to its trapping mechanism.

In conclusion, delayed iodoDPA SPECT imaging of C57bl/6 and ApoE -/- mice revealed focal vascular and myocardial uptake of radiotracer within individual phenotypic atherosclerotic mice consistent with their genotype. Addition of HFHC diet increased plaque burden on average and iodoDPA SPECT correctly revealed the plaque distribution within individual mice, showing variation in plaque burden among ApoE -/- mice on a normal or HFHC diet. The SPECT results correlated with findings on echocardiography and histology providing initial validation of iodoDPA as a viable, new imaging agent for atherosclerosis.

Sources of funding

Sibley Memorial Hospital Mackley Fund (CAF), Lupus Foundation of America, R01 EB009367 (MGP), PO-1HL-107153-01 (SC).

Conflict of interest

The authors have no relevant conflicts of interest.

Acknowledgments

We acknowledge Gilbert Green for performing SPECT scans and Oscar Cingolani, M.D. for a critical review of this manuscript.

Appendix A. Supplementary data

Supplementary data related to this article can be found at http://dx.doi.org/10.1016/j.bbrc.2015.03.171.

Transparency document

Transparency document related to this article can be found online at http://dx.doi.org/10.1016/j.bbrc.2015.03.171.

References

[1] K.S. Reddy, S. Yusuf, Emerging epidemic of cardiovascular disease in developing countries, Circulation 97 (1998) 596–601.
[2] The World Health Report, Making a difference, Salud Publica De Mexico, 41, 1999, pp. 254–256.
[3] M. Mizobuchi, D. Towler, E. Slatopolsky, Vascular calcification: the Killer of patients with chronic kidney disease, J. Am. Soc. Nephrol. 20 (2009) 1453–1464.
[4] P.A. Calvert, T.V. Liew, I. Gorenne, M. Clarke, C. Costopoulos, D.R. Obaid, M. O'Sullivan, L.M. Shapiro, D.C. McNab, C.G. Densem, P.M. Schofield, D. Braganza, S.C. Clarke, K.K. Ray, N.E.J. West, M.R. Bennett, Leukocyte telomere length is associated with high-risk plaques on virtual histology intravascular ultrasound and increased proinflammatory activity, Arterioscler Thromb Vasc. Biol. 31 (2011) 2157–U2580.

[5] T.A. Wynn, L. Barron, Macrophages: master regulators of inflammation and fibrosis, Semin. Liver Dis. 30 (2010) 245–257.
[6] L.L. Demer, Y. Tintut, Vascular calcification: pathobiology of a multifaceted disease, Circulation 117 (2008) 2938–2948.
[7] J.C. Wang, M. Bennett, Aging and atherosclerosis: mechanisms, functional consequences, and potential therapeutics for cellular senescence, Circ. Res. 111 (2012) 245–259.
[8] F. Bonomini, S. Tengattini, A. Fabiano, R. Bianchi, R. Rezzani, Atherosclerosis and oxidative stress, Histol. Histopathol. 23 (2008) 381–390.
[9] N. Kume, T. Murase, H. Moriwaki, T. Aoyama, T. Sawamura, T. Masaki, T. Kita, Inducible expression of lectin-like oxidized LDL receptor-1 in vascular endothelial cells, Circulation Res. 83 (1998) 322–327.
[10] M.P. Ramprasad, W. Fischer, J.L. Witztum, G.R. Sambrano, O. Quehenberger, D. Steinberg, The 94-Kda to 97-Kda mouse macrophage membrane-protein that recognizes oxidized low-density-lipoprotein and Phosphatidylserine-rich liposomes is identical to macrosialin, the mouse homolog of human Cd68, Proc. Natl. Acad. Sci. U. S. A. 92 (1995) 9580–9584.
[11] K.M. Kelly, P.M. Tarwater, J.M. Karper, D. Bedja, S.E. Queen, R.S. Tunin, R.J. Adams, D.A. Kass, J.L. Mankowski, Diastolic dysfunction is associated with myocardial viral load in simian immunodeficiency virus-infected macaques, AIDS 26 (2012) 815–823.
[12] D.M. Poitz, A. Augstein, S. Weinert, R.C. Braun-Dullaeus, R.H. Strasser, A. Schmeisser, OxLDL and macrophage survival: essential and oxygen-independent involvement of the Hif-pathway, Basic Res. Cardiol. 106 (2011) 761–772.
[13] P.R. Moreno, A. Kini, Resolution of inflammation, statins, and plaque regression, JACC Cardiovasc Imaging 5 (2012) 178–181.
[14] D. Li, A.R. Patel, A.L. Klibanov, C.M. Kramer, M. Ruiz, B.Y. Kang, J.L. Mehta, G.A. Beller, D.K. Glover, C.H. Meyer, Molecular imaging of atherosclerotic plaques targeted to oxidized LDL receptor LOX-1 by SPECT/CT and magnetic resonance, Circ. Cardiovasc. Imaging 3 (2010) 464–472.
[15] S. Tsimikas, Noninvasive imaging of oxidized low-density lipoprotein in atherosclerotic plaques with tagged oxidation-specific antibodies, Am. J. Cardiol. 90 (2002) 22L–27L.
[16] K. Nishigori, T. Temma, K. Yoda, S. Onoe, N. Kondo, M. Shiomi, M. Ono, H. Saji, Radioiodinated peptide probe for selective detection of oxidized low density lipoprotein in atherosclerotic plaques, Nucl. Med. Biol. 40 (2013) 97–103.
[17] A.M. Scarf, M. Kassiou, The translocator protein, J. Nucl. Med. 52 (2011) 677–680.
[18] N. Van Camp, R. Boisgard, B. Kuhnast, B. Theze, T. Viel, M.C. Gregoire, F. Chauveau, H. Boutin, A. Katsifis, F. Dolle, B. Tavitian, In vivo imaging of neuroinflammation: a comparative study between [F-18]PBR111, [C-11] CLINME and [C-11]PK11195 in an acute rodent model, Eur. J. Nucl. Med. Mol. Imaging 37 (2010) 962–972.
[19] F. Chauveau, N. Van Camp, F. Dolle, B. Kuhnast, F. Hinnen, A. Damont, H. Boutin, M. James, M. Kassiou, B. Tavitian, Comparative evaluation of the translocator protein radioligands 11C-DPA-713, 18F-DPA-714, and 11C-PK11195 in a rat model of acute neuroinflammation, J. Nucl. Med. Official Publ. Soc. Nucl. Med. 50 (2009) 468–476.
[20] L.H. Lash, T.M. Visarius, J.M. Sall, W. Qian, J.J. Tokarz, Cellular and subcellular heterogeneity of glutathione metabolism and transport in rat kidney cells, Toxicology 130 (1998) 1–15.
[21] A. Batarseh, V. Papadopoulos, Regulation of translocator protein 18 kDa (TSPO) expression in health and disease states, Mol. Cell. Endocrinol. 327 (2010) 1–12.
[22] X. Qi, J. Xu, F. Wang, J. Xiao, Translocator protein (18 kDa): a promising therapeutic target and diagnostic tool for cardiovascular diseases, Oxid. Med. Cell. Longev. 2012 (2012) 162934.
[23] F.S. Foster, C.J. Pavlin, K.A. Harasiewicz, D.A. Christopher, D.H. Turnbull, Advances in ultrasound biomicroscopy, Ultrasound Med. Biol. 26 (2000) 1–27.
[24] X.P. Yang, Y.H. Liu, N.E. Rhaleb, N. Kurihara, H.E. Kim, O.A. Carretero, Echocardiographic assessment of cardiac function in conscious and anesthetized mice, Am. J. Physiology Heart Circulatory Physiol 277 (1999) H1967–H1974.
[25] I. Wendelhag, T. Gustavsson, M. Suurkula, G. Berglund, J. Wikstrand, Ultrasound measurement of wall thickness in the carotid artery: fundamental principles and description of a computerized analysing system, Clin. Physiol. 11 (1991) 565–577.
[26] H. Wang, M. Pullambhatla, T.R. Guilarte, R.C. Mease, M.G. Pomper, Synthesis of [(125)I]iodoDPA-713: a new probe for imaging inflammation, Biochem. Biophysical Res. Commun. 389 (2009) 80–83.
[27] D. Fairweather, M.J. Coronado, A.E. Garton, J.L. Dziedzic, A. Bucek, L.T. Cooper Jr., J.E. Brandt, F.S. Alikhan, H. Wang, C.J. Endres, J. Choi, M.G. Pomper, T.R. Guilarte, Sex differences in translocator protein 18 kDa (TSPO) in the heart: implications for imaging myocardial inflammation, J. Cardiovasc. Transl. Res. 7 (2014) 192–202.
[28] A.M. Allen, J.M. Taylor, A. Graham, Mitochondrial (dys)function and regulation of macrophage cholesterol efflux, Clin. Sci. 124 (2013) 509–515.
[29] S. Cinti, Between brown and white: novel aspects of adipocyte differentiation, Ann. Med. 43 (2011) 104–115.
[30] A. Giordano, I. Murano, E. Mondini, J. Perugini, A. Smorlesi, I. Severi, R. Barazzoni, P.E. Scherer, S. Cinti, Obese adipocytes show ultrastructural features of stressed cells and die of pyroptosis, J. Lipid Res. 54 (2013) 2423–2436.
[31] C.A. Foss, J.S. Harper, H. Wang, M.G. Pomper, S.K. Jain, Noninvasive molecular imaging of tuberculosis-associated inflammation with radioiodinated DPA-713, J. Infect. Dis. 208 (2013) 2067–2074.
[32] F. Chauveau, H. Boutin, N. Van Camp, F. Dolle, B. Tavitian, Nuclear imaging of neuroinflammation: a comprehensive review of [11C]PK11195 challengers, Eur. J. Nucl. Med. Mol. Imaging 35 (2008) 2304–2319.
[33] G. Pottier, N. Bernards, F. Dolle, R. Boisgard, [18F]DPA-714 as a biomarker for positron emission tomography imaging of rheumatoid arthritis in an animal model, Arthritis Res. Ther. 16 (2014) R69.
[34] X. Shao, X. Wang, S.J. English, T. Desmond, P.S. Sherman, C.A. Quesada, M.R. Piert, Imaging of carrageenan-induced local inflammation and adjuvant-induced systemic arthritis with [(11)C]PBR28 PET, Nucl. Med. Biol. 40 (2013) 906–911.
[35] F. Pugliese, O. Gaemperli, A.R. Kinderlerer, F. Lamare, J. Shalhoub, A.H. Davies, O.E. Rimoldi, J.C. Mason, P.G. Camici, Imaging of vascular inflammation with [11C]-PK11195 and positron emission tomography/computed tomography angiography, J. Am. Coll. Cardiol. 56 (2010) 653–661.
[36] G. Tegler, J. Sorensen, K. Ericson, M. Bjorck, A. Wanhainen, 4D-PET/CT with [(11)C]-PK11195 and [(11)C]-(D)-deprenyl does not identify the chronic inflammation in asymptomatic abdominal aortic aneurysms, Eur. J. Vasc. Endovasc. Surg. 45 (2013) 351–356.